above which the low-frequency oscillation will dominate, we can take $Ro_* = c/\omega R$ (c is the maximum phase velocity of the axisymmetric wave: $c = 0.52\omega R$ [4]).

The experimental results show that the vortices were created by the normal inertial oscillations, as in [1]. The only difference is that in [1] the oscillation was excited by resonant "pumping" of effectively a single mode, whereas the flow generated after pulling bodies through the rotating liquid in general has the features of a large number of modes differing in geometry and frequency. This was graphically shown by experiments in which disks of diameter 5 and 10 cm were pulled along the axis of the container at large Ro. A sharply defined beat was observed at the cyclone vortex generated in the region near the axis. The experimental frequency Ω was close to half the sum of the frequencies of the modes (0, 1, 1) and (0, 2, 1) and was lower than for a disk of diameter 7 cm.

Finally we note that, for the intervals of the parameters studied in our experiments, the flow field did not depend on Re.

LITERATURE CITED

1. V. G. Makarenko and V. F. Tarasov, "Experimental model of a tornado," Zh. Prikl. Mekh. Tekh. Fiz., No. 5 (1987).
2. Lord Kelvin, "Vibrations of a columnar vortex," Philos. Mag., 10 (1880).
3. Kh. Grinspen, Theory of Rotating Fluids [in Russian], Gidrometeoizdat, Leningrad (1975).
4. G. K. Batchelor, An Introduction to Fluid Dynamics, Cambridge University Press (1973).

VARIOUS APPROXIMATIONS IN THE THEORY OF CAVITATION FLOWS OF A VISCOUS CAPILLARY FLUID

E. L. Amromin, A. V. Vasil'ev, and V. V. Droblenkov

The purpose of calculating cavitation flows is usually the search of cavity sizes and pressure distributions over streamlined bodies. Most of these calculations are carried out within mechanics of an ideal fluid. However, a number of experimental facts – the presence of a separation boundary layer [1] and a dilatation zone [2] on the body in front of the cavity, the effect of body sizes and its stream velocity on hydrodynamic reactions, cavity sizes [3, 4], and even their existence – require study of the effect of the viscosity of the fluid and its surface tension on cavitation streamline flows of various types.

The pressure diagram for a body with a cavity is determined by the external inviscid flow. The presence of viscosity leads to substantial deviation of the current line from the surfaces of the body and the cavity in three zones: in front of the cavity, behind it, and near the intake extremity of the body. The pressure diagram at the body within these zones also differs substantially from the pressure diagram at a body with a cavity in an ideal fluid. The feature flows in the first two zones are illustrated by Fig. 1: curves 1 and 2 are the cavity boundaries in an ideal and in a viscous capillary fluid for the same σ value – the cavitation number; 3 and 4 are the corresponding calculated pressure diagram coefficient C_p at the streamline of a body with a cap [1], part of whose meridional cross section contour is illustrated by curve 5; $\sigma = 2(p_\infty - p_c)\rho^{-1}V_\infty^{-2}$; $C_p = 2(p - p_\infty)\rho^{-1}V_\infty^{-2}$; ρ is the fluid density, V_∞ is the flow velocity; p_∞ is the pressure in it; and p_c and p are the pressures in the cavity and at an arbitrary point of the boundary between the inviscid and viscous flows. Curves 1-4 are the calculated ones, with $\sigma = 0.36$. For an ideal fluid the calculations were carried out by using the generalized Ryabushinskii scheme with closure of the cavity frequency at the edge (whose meridional cross section is illustrated by segment 6), as was done numerically in [3]. For a viscous capillary fluid the calculations were carried out by the method used in [5] for values of the Reynolds number $Re = 10^6$ and a Weber number $We = 2\cdot10^5$ for vanishing value of the boundary angle, i.e., for an absolutely wettable body; Re and $We = \rho V_\infty^2 D\gamma^{-1}$ are constructed by the same characteristic size D (the diameter of a

Leningrad. Translated from Zhurnal Prikladnoi Mekhaniki i Tekhnicheskoi Fiziki, No. 6, pp. 117-126, November-December, 1988. Original article submitted August 20, 1987.

0021-8944/88/2906-0874$12.50

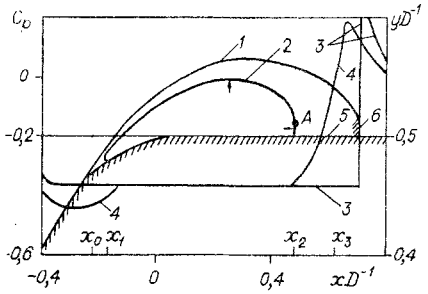

Fig. 1

body of revolution or the chord length for the profile), γ is the surface tension coefficient at the boundary between the fluid and the gas, x_0 is the abscissa of the opening zone ahead of the cavity, and x_1 and x_2 are the abscissas of the opening and rear of the cavity.

The first zone of a viscous– inviscid interation is formed by the simultaneous effect of viscosity and surface tension. A cavity in a real fluid has a nonvanishing width at the line attached to the body, and, similarly, generates a break in the boundary layer ahead of it.

The second zone precedes the boundary layer associated with the body: at its end the cavity has a nonvanishing thickness too, which is related to the presence of an opposite stream at the edge of the real cavity. In the scheme described here it has been taken into account that the real cavity located inside the boundary layer is penetrable for the fluid. Therefore, the fluid flow averaged over time is directed inside the cavity at the rear part of its boundary (propagating from point A on curve 2 to the wall) and from the cavity through the remaining portion of the boundary (as shown by arrows in Fig. 1). This flow inside the boundary layer does not change the conditions at the boundary between them and the external inviscid flow, and does not lead to violation of the mass conservation law for flow as a whole.

The third zone of strong viscous–inviscid interaction near the stern of the body is investigated neither in [5] nor in the present study. It also exists in cavitationless flows [6], its effect on cavitation can be indirect, and is primarily manifested in terms of variations in the pressure and buoyant force distributions.

Calculations of cavitation flows of a viscous fluid involve both substantial computational difficulties and the necessity of using semiempirical dependences, sometimes based on very few experiments and on long successive estimates. Therefore, it is important to verify the simplified schemes and the methods of calculating cavitation streamline flows of a viscous fluid.

The purpose of the present study is analysis of the latter simplifications, related to incomplete account of the viscous–inviscid interaction and to the assumption of a thin cavity. The analysis is advisably started with a more detailed description than given in [5, 7, 8] of the method used for calculations of cavitation streamline flows of a viscous fluid, i.e., for solutions of the following problem: the fluid is homogeneous, weightless, and incompressible, the flow is steady, planar or axially symmetric, the pressure in the cavity is constant, the cavity position in the body is assigned, i.e., the abscissas of its origin and its end x_1, x_2, as well as the Re value, the turbulence of the leading flow [9], and the dependence on wettability of the streamline boundary angle [3, 7]. It is required to find the shape of a cavity corresponding to σ and We values, as well as the pressure on the surface of the streamlined body.

The pressure in the cavity is related to the pressure in the fluid by the Laplace equation

$$C_p + \sigma = 2\varkappa D \mathrm{We}^{-1} \tag{1}$$

($\varkappa$ is the curvature of the cavity boundary). The boundaries of the cavity and of the inviscid flow coincided within mechanics of an ideal fluid; for the scheme of cavity enclosure selected the latter was determined from the boundary value problem for the velocity potential Φ, since C_p is related to the components of grad Φ by the Bernoulli integral; in this case the cavity shape is sought at the same time. In a viscous fluid the boundaries mentioned are separated by a boundary layer, and the pressure at the cavity boundary is related

to the absolute value of the velocity of inviscid flow on the displaced body. The surface cross section S* can be obtained primarily by the streamline increment of the body and the cavity at the displacement thickness δ^*. Similarly to the cavity boundary in an ideal fluid, the surface of the displaced body can be determined in calculating the inviscid flow, since it is part of the free boundary. Assigning on this boundary a velocity distribution f(S), denoting by R the distance from S* to the streamlined body, by s_0, s_1, s_2, s_3 the arc coordinates on S* of the points having abscissas x_0, x_1, x_2, x_3, and by N and T the unit external normal and tangent to S*, one can formulate the following nonlinear problem with the purpose of searching R and the derivatives of Φ, written down with the use of quantities depending on the boundary layer characteristics:

$$\Delta\Phi = 0; \tag{2}$$

$$\partial\Phi/\partial N \mid_{S^*} = 0; \tag{3}$$

$$\partial\Phi/\partial T \mid_{s\in(s_0, s_3)} = -f(s); \tag{4}$$

$$R(s_0) = \delta^*(s_0); \tag{5}$$

$$dR(s_3)/dT = d\delta^*(s_3)/dT; \tag{6}$$

$$dR(s_0)/dT = d\delta^*(s_0)/dT; \tag{7}$$

$$|\text{grad } \Phi| \to V_\infty, \; x^2 + y^2 \to \infty. \tag{8}$$

Here {x, y} are the Cartesian coordinates of planar flow (a half-plane of meridional cross section flow). The necessity of finding R from f values is related to the fact that neither the cavity shape nor the displacement on it are known ahead of time. The problems of calculating the cavitation flow of an ideal fluid (2)-(8) are distinguished by the shape of the right-hand sides of Eqs. (4)-(7). To solve the problem (2)-(8) it is necessary to assign the values of δ^*, $d\delta^*/dT$ for $s = s_0$ and $s = s_3$, as well as the function f(s) within a single undetermined coefficient C_0 [as in mathematical problems of ideal cavitation similar to (2)-(8)]. However, δ^*, $d\delta^*/dT$, s_0, s_3, and f are unknown ahead of time, and depend on the boundary layer characteristics. The function f(s) which, according to experimental data, must have two portions decreasing over the separating zones and be practically constant over a large portion of the cavity (since there $|\varkappa D| \sim 1$, and usually $We \gg 100$), can be approximated by a linear combination of given functions f_1, f_2 and undetermined coefficients $f(s) = C_0 + C_1 f_1(s) + C_2 f_2(s)$. The functions f_1, f_2 are nonvanishing only within the first and second strong interactions, respectively, while their shapes are selected on the basis of analyzing experimental data on pressure distributions. The undetermined coefficients C_2, C_1, $C_0 \equiv (1 + \sigma)^{0.5}$ therefore depend implicitly on the lengths of the viscous separation zones.

The boundary layer from the critical point to s_0 can be calculated by one of the known methods, such as that described in [9]. The values of δ^* and of the width of pulse loss δ^{**} are extrapolated through the first strong interaction zone by means of the Squire–Young equation to the point $s = s_1'$, where $f = C_0$, and one uses $v_0 = u_0 = 0$ (u_0, v_0 are the components of fluid velocity at the cavity boundary). The boundary layer over the cavity is described by means of three relations: the van Karman equation

$$U^2 d\delta^{**}/dT + v_0(U - u_0) = 0; \tag{9}$$

the Prandtl equation for the cavity boundary, being a surface of vanishing friction,

$$u_0 du_0/dT = a(U - u_0)^3/u\delta^* \tag{10}$$

and the longitudinal profile of the velocity component of the turbulent boundary layer, used in calculations of separated flows [6]

$$u(\eta) = u_0 + (U - u_0)(3\eta^2 - 2\eta^3). \tag{11}$$

Here η is the coordinate precipitated from the cavity boundary along the normal and referring to the width of the boundary layer; and a = const. To find δ^* and δ^{**} from system (9)-(11), integrating it from the point $s = s_1'$, one must know not only $U = -\partial\Phi/\partial T$, but also v_0. The v_0 values are related to the time-averaged intensity of the inverse jet, and, consequently,

with c $[\delta^*]$ – the jump in δ^* at $x = x_2$ ($s = s_2$); in planar flow, in particular, $\int_{s_1'}^{s_2} v_0 ds = C_0 [\delta^*]$.

The simplest shape was selected for v_0 calculations: $v_0 = C_3(s - s_1')$, $C_3 = \text{const}$. The s_1' and We values are determined in integrating (1) over the ordinates of the cavity boundary y_c: this second-order ordinary differential equation in y_c having four conditions, assigning y_c and dy_c/dT at $s = s_1$ and $s = s_1'$, due to which two parameters can be selected in the calculations. For $s > s_2$ δ^* is determined from (5), following which $[\delta^*]$ is found.

The four decisive quantities C_1, C_2, s_0, s_3 are sought from local semiempirical separation conditions and the associated boundary layer, corrected with the purpose of accounting for the effect of the large curvature of the flow boundaries in finite cavities and the associated high transverse velocities in the boundary layer, as well as from the continuity condition of dU/dT for $s = s_0$. These conditions are [5, 6]

$$\frac{\delta^*}{U}\frac{dU}{dT}\Big|_{s_3} = -0.015; \tag{12}$$

$$\frac{[B^* - \delta^*(s_3)]^{1.25}[\delta^*(s_2 + 0)]^{0.25}}{[s_2 - s_1']^{0.5}(s_3 - s_2)} = \frac{1}{12}; \tag{13}$$

$$\frac{dU}{dT} + 1{,}1\frac{UD}{\delta^* \mathrm{Re}} - UD^{3.5}\left(\mathrm{We}\,U\frac{dU}{dT}\right)^{0.67}\frac{(s_1 - s_0)^{2.33}}{5}\Big|_{s_0} = 0; \tag{14}$$

$$\frac{dU}{dT}(s_0 + 0) = \frac{dU}{dT}(s_0 - 0), \tag{15}$$

where B^* is the maximum cavity width, i.e., the difference between y_c and the body ordinates. Condition (14) was derived for a laminar layer in front of the cavity. For a turbulent layer (14) is replaced by the condition $s_1 = s_0 + 2\delta^*(s_0)$ [5]. The criteria (13), (14), introduced and used for the small number of presently known experimental data on boundary layers in cavitation flows, can be refined in the following.

Due to the nonlinearity of system (1)-(15), the calculations must be carried out by multiple-level successive approximations, whose convergence is analyzed by the inviscid values in condition (4), as well as by the convergence of successive values of σ and log We, obtained within these approximations.

Each approximation of the upper level consists of calculating the streamline potential of a displaced body of given shape, calculating the boundary layer, and of correcting the shape of the displaced body over the cavity and strong interaction zones. Within the first approximation U is determined in two stages: initially directly on the surface of the streamlined body (by the method of [3]), while for the profile one takes into account the effect of Re on the value of the buoyant force coefficient (by means of the correction to the C_y value described in [10], p. 126, satisfying the Zhukovskii–Chaplygin postulate); then, within the first approximation (and only then), to partially account for the cavity effect on the pressure gradient in the boundary layer in front of it, U is increased by δU:

$$\delta U(s) = \frac{1}{\pi}\int_{s_1}^{s_2}\frac{q(\xi)}{s - \xi}\,d\xi; \tag{16}$$

$$q(s) = \frac{F(s)}{\pi}\int_{s_1}^{s_2}\frac{U(\xi)\,d\xi}{(s - \xi)F(\xi)}. \tag{17}$$

Here $F(s) = (s - s_1)^{0.5}(s_2 - s)^{0.5}$. Since (17) is used only for arcs (s_1, s_2), the problem of behavior of F(s) at infinity is unimportant here. Equations (16), (17) determine the induction from a thin cavity, located on a body of arbitrary thickness and simulated by the Zhukovskii–Roshko scheme (or a scheme similar to it) in an ideal fluid. The corresponding boundary displacement of potential flow is sought from the equation

$$q + \frac{d}{dT}(RU) = 0 \tag{18}$$

with the initial condition $R(s_1) = 0$. The calculation of the boundary layer on the basis of one of the methods described in [9] can be done nonuniquely within each approximation, since the s_0 value is found from condition (14), containing the We value refined in the calculation process. Simultaneously with s_0, C_1 is determined from (15).

To find s_3 from (13) it is necessary to know the cavity shape. Assigning a trial value of s_3, from Eqs. (6), (12) one must seek C_0 and C_2, for which conditions (3), (4) are linearized on the boundary of the inviscid flow used for the calculation of U for $s \in (s_0, s_3)$:

$$\frac{\partial \Phi}{\partial T}(q^*) + C_0 + C_1 f_1 + C_2 f_2 = U; \tag{19}$$

$$q^* + 2\frac{d}{dT}(Ur) = 0, \tag{20}$$

where r is unknown perturbation in R, which must be determined by eliminating from Eqs. (19) and (20) the primarily low potential density q^*. It is convenient to represent $\partial\Phi/\partial T(q^*)$ in the form of the sum $\partial\Phi/\partial T(q^*) = \partial\varphi_1/\partial T + \partial\varphi_2/\partial T + J$ where the first term includes the contribution of the variation δ^* of the boundary layer to $\partial\Phi/\partial T$ on S* for $s \in (s_0, s_3)$, and the remaining two terms are the perturbation $\partial\Phi/\partial T$ with respect to the variation in the ordinates of the displacement body for $s > s_0$. The function J is the Cauchy integral of the density $q^*/2$, while the derivative $\partial\varphi_2/\partial T$ for a planar, weakly twisted boundary is negligibly small in comparison with the remaining terms. Relationship (19) is a singular integral equation determining the function $q^*(s)$ on the interval (s_0, s_3). The Cauchy integral is transformed so as to eliminate q^*, which is possible when the boundedness condition of q^* on (s_0, s_3) is satisfied:

$$\pi C_0 = \int_{s_0}^{s_3} \frac{U(\xi) - C_1 f_1(\xi) - C_2 f_2(\xi) - \frac{\partial\varphi_1}{\partial T}(\xi) - \frac{\partial\varphi_2}{\partial T}(\xi, q^*)}{[(\xi - s_0)(s_3 - \xi)]^{0.5}} d\xi. \tag{21}$$

Condition (21) satisfies relations (6), (7), and makes it possible to express C_0 in terms of q^* and C_2. Therefore r, determined by integrating (20) with the initial condition (5), is a linear function of one undetermined coefficient C_2: $r(s_3) = \alpha_1 + \alpha_2 C_2$ (α_1, α_2 are constants). To calculate C_2, we assume ahead of time equality of δ^* and R + r for $s = s_3$, and then (12) acquires the form:

$$(R + \alpha_1 + \alpha_2 C_2) C_2 df_2/dT + 0.015(C_0 + C_2 f_2) = 0. \tag{22}$$

In what follows we use the smaller root of this quadratic equation in C_2.

Following the determination of C_2 and, consequently, f and r, one can verify condition (13) and correct the s_3 value. If (13) is satisfied, then to calculate δ^* and δ^{**} for $s > s_0$ one uses U = f; the necessity of iterations in finding δ^* and δ^{**} is related to the determination of $[\delta^*]$, since $v_0 \sim [\delta^*]$. Calculations within each approximation determine y_c from the R and δ^* values for $s \in (s_1', s_2)$.

As an example of using the method described we show in Fig. 2 a comparison of plotted measurements of the experimental data of [11] with an indicated measurement spread for an 8% symmetric profile with a parabolic tip for $Re = 1.5 \cdot 10^6$ with results of the dependences, with the calculated curve and the experimental results 1 corresponding to an attack angle $\alpha = 4.2°$, $2 - \alpha = 6.3°$, while 1a are the results of calculating ideal cavitation for $\alpha =$ 4.2°. The abscissa x_2 in the dependences of Fig. 2 is traced along the chord from the leading edge of the profile. Comparing these curves, it can be concluded that: to realize for the same α in a viscous fluid at a given profile a cavity of the same length as in the ideal case, it is necessary to enhance the angle of attack by nearly 1.5 times.

The agreement between the calculated dependences 1 and 2 and experiment is better, but the computational procedure suggested is quite complicated: four-level approximations are used (to refine σ, We, s_3, and $[\delta^*]$) for given $\{x_1, x_2\}$. For engineering calculations, in which it is usually required to assign not $\{x_1, x_2\}$, but $\{\sigma, We\}$, it is still necessary to select $\{x_1, x_2\}$ by successive approximations. Therefore, the analysis of simplified versions of the theory is quite important. One of them was sufficiently effective for calculations of supercavities behind bodies with smooth enclosures [7]; the boundary layer characteristics in it were calculated only up to $s = s_1'$, and their further variation was assumed to weakly affect the cavity sizes, for whose enclosure we used the generalized Ryabushinskii

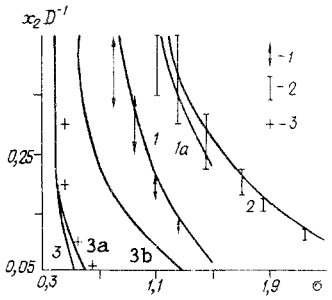

Fig. 2

scheme which is traditional in ideal cavitation. We further consider another simplification of the theory suggested, where in all calculations we put $a = 0.03$ and $d\delta^*/dT(s_3) = 0$ in Eq. (10).

When the body with cavitationless streamlines has a sharp and deep minimum of C_p, the position of the points s_0, s_1 is slightly changed with varying We and σ. Therefore, the effect of We on the cavity sizes drops sharply with increasing x_2 or s_2. This statement illustrates the results for a 4% segment profile at $\alpha = 2°$, shown in Fig. 2. The calculated curve 3 and the experimental points of [12] correspond to $Re = 10^6$, $We = 10^5$, curve 3a to $Re = 10^6$, $We = 2 \cdot 10^4$, and curve 3b is the calculation of ideal cavitation with the use of the generalized Ryabushinskii scheme. The insignificant difference in cavity sizes even for $x_2D^{-1} > 0.1$ for We values differing by 5 times implies a weak effect on these sizes of the first strong interaction zone. In similar cases the flow analysis in this zone (following the iteration level in the calculations) can be omitted.

One more possibility of simplifying the calculations is related to the use of the assumption of a thin cavity. For these cavitities

$$B^* \ll x_2 - x_1 \tag{23}$$

and, since the surfaces of the displacement body and of the streamlined body are close to each other, it seems admissible to restrict the treatment to a single external approximation in the problem and to single refinement of U by only one of Eqs. (16), (17). Omitting the relatively low-effect term $\partial\varphi_2/\partial T$ in (19), (21), this approximation can be considered quasiplanar and quasilinear. Among them the Neumann problem (2), (3), (8) is solved within the exact statement for a streamlined body of three-dimensional flow; in particular, the cavitation calculation is carried out for a planar, weakly twisted beam in an inhomogeneous flow. In this approach it seems necessary to use only one approximation of the external level. The large computational advantages of the quasiplanar quasilinear approach in computer calculations are related to the fact that their most difficult part, the solution of the exterior Neumann problem, is possible to carry out only once for all the pairs of $\{x_1, x_2\}$ values used, while for fixed C_y – this is also possible for all Re values, which, in comparison with the nonlinear theory, can cut on computer time by many times (depending on the number of variants: the higher the number of variants, the higher the economy in time).

It must be shown, however, where this simplification leads. Comparison of the quasiplanar quasilinear and nonlinear theories for two bodies of revolution with substantial elongation with different front edges is shown in Fig. 3. Curves 1, 2 were calculated for a body with a hemispherical front edge: line 1 corresponds to the quasilinear quasiplanar theory for $Re = 10^7$, 1a is the nonlinear theory for the same Re, and 1b is the nonlinear theory for an ideal fluid (when using the generalized Ryabushinskii scheme). Also shown are the results for a body with a Swedish [1] front cap, already illustrated in Fig. 1; the solid lines show the dependences on the cavitation number ratio x_2D^{-1}, while the dashed 2, 2b show the dependence on σ of the ratio of cavity width B to the diameter of the body. Curves 2 correspond to the quasiplanar quasilinear theory for a viscous fluid with $Re = 10^6$, $We = 2 \cdot 10^5$, curve 2a – the nonlinear theory for the same Re and We values, and curve 2b – the nonlinear theory for an ideal fluid. For $B(\sigma)$ the nonlinear and quasilinear theories provide for a viscous fluid coinciding results within the scale of Fig. 3. The origin of coordinates for bodies of revolution coincides with the origin of the cylindrical part, while $x_1 < 0$ for all $\{\sigma$, Re, We$\}$. It can be established from the curves of Fig. 3 that the cavities considered indeed satisfy condition (23). However, both the use of planar cross section and quasilinearization are capable of enhancing σ for $x_2 = \text{const}$, which is also explained by the mutual position of lines 1 and 1a, as well as 2 and 2 .

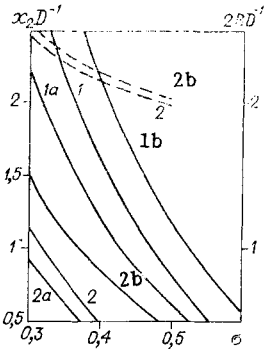

Fig. 3

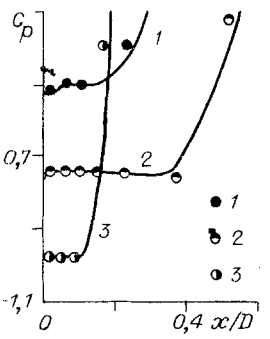

Fig. 4

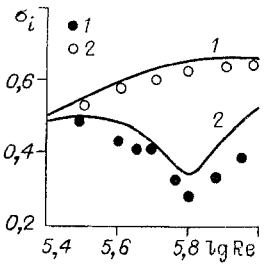

Fig. 5

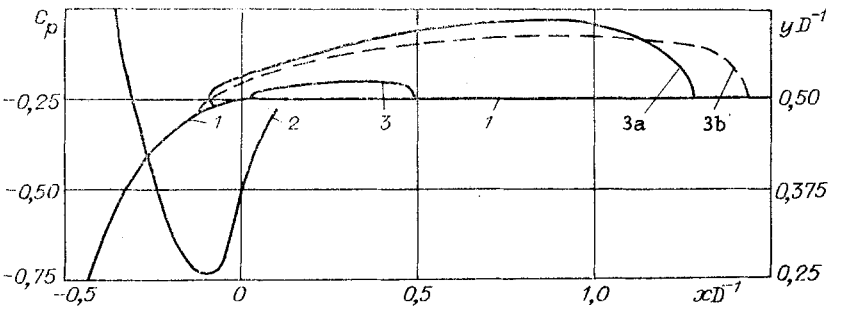

Fig. 6

The results represented in Fig. 3 imply that the quasiplanar quasilinear theory makes it possible to take into account the basic role of the effect of We and Re on the sizes of relatively short cavities. For large deviations of both versions from ideal cavitation of bodies of revolution these deviations are comparable with the measurement spread from the quite effective simpler theory – ideal cavitation. For cavities on planar profiles the dependences $x_2(\sigma, \alpha)$ differ substantially in an ideal and viscous capillary fluid for any σ. However, for long cavities ($x_2D^{-1} \to 0.5$) a significant part of this deviation can be removed by introducing the correction to effect of Re recommended in [10] into the dependence $C_y(\alpha)$. By using these corrections it is possible to reach satisfactory agreement with experiment not only in the cavity sizes, but also in finer characteristics, such as the distribution of C_p on parts of the body close to the cavity. This assertion is verified by the comparisons shown in Fig. 4 between C_p measurements [13] on a Valkhner-7 profile with a chord length D = 0.08 m at Re $\approx 10^6$ and the calculated curves. Curve and point 1 correspond to $\alpha = -2°$, and curves and points 2 and 3 – to $\alpha = 3°$ for different σ. Finally, it must be noted that even the quasiplanar quasilinear theory makes it possible to explain complicated physical effects related to the effect of viscosity and capillarity on cavitation, such as the Arakeri–Acosta effect [4].

According to the long practice of observing development of cavitation, the cavities grow on well-streamlined bodies for any method of reducing σ. Contradictory experiments [4] appeared in this practice: when a body with a hemispherical front cap of diameter D = 0.05 m was established as turbulizer, and for values Re $\approx 2 \cdot 10^5$ and $\sigma \approx 0.45$ a cavity was observed on it, but with increasing flow velocities, accompanied by reduction in σ, the cavity initially decreases and then vanishes altogether. Unusual for a body with a turbulizer is also an Re dependence of characteristic appearance of cavities on the body of critical cavitation number σ_i. This dependence is represented by the experimental points 1 in Fig. 5, and points 2 – the results of σ_i measurements on the same body without a turbulizer.

The theory discussed can be used for determining σ_i in flows with low gas content: the dependence of σ on the cavity length for fixed Re and We in stationary flows due to the effect of capillarity has a maximum for $x_2 - x_1 > 0$; it is also used as σ_i for cavities associated to the body both in contemporary experiments [4] and in calculations [8]. Results of calculating σ_i by the quasiplanar quasilinear theory are shown by lines 1 and 2 in Fig. 5. The presence of a turbulizer was accounted for in the calculations by assigning the origin of the laminar-turbulent transition zone on the body at assigned points. Since even for a

body with a turbulizer there is reasonable agreement between calculations and experiments, on the basis of these calculations one can explain the Arakeri–Acosta effect.

On the front part of the body used in experiment [4] there occurs a mild pressure minimum (part of the meridional cross section of this body is illustrated by curve 1 in Fig. 6, and 2 is part of the C_p diagram for cavitationless streamlines of this body). Below the flow and from the minimum of C_p there occurs an increase in dC_p/dT. For relatively low Re, despite the presence of the turbulizer the boundary layer in front of the cavity remains laminar, and its dominant zone of viscous separation remains in equilibrium only in regions of small positive dC_p/dT, i.e., near the minimum of C_p. For higher Re the cavity is completely located in a turbulent boundary layer and the origin of the separation zone must correspond to larger dC_p/dT, which, as shown by calculations, for corresponding experimental conditions [4] cannot be generated by the inverse cavity effect on C_p in front of it. Therefore, for the body considered in a turbulent boundary layer the cavities must be displaced toward below the flow, into the high-pressure zone, as shown in Fig. 6, where curves 3-3b plot the cavity boundaries for the same value of $\sigma = 0.3$, while boundary 3 corresponds to $Re = 5 \cdot 10^5$, $D = 0.05$ m on a body with a turbulizer, 3a – the same Re and D values for a body without a turbulizer, and line 3b – $Re = 10^7$, $D = 1$ m, i.e., the same conditions as for curves 1 and 1a in Fig. 3.

Due to the effects mentioned above, for the same $\{\sigma, Re, We\}$ values one can observe cavitation on a body without a turbulizer, as well as its vanishing in its presence. For further increase in Re, since for the same body one must not vary Re and We independently, due to which with increasing Re there is incidental thinning of principal portions and a decrease in minimal cavity lengths, the cavities can appear above the flow in the zone of smaller C_p (see Fig. 6), while the dependence of $\sigma_i(Re)$ is again increasing and, as seen from Fig. 3, cavitation also exists for $\sigma > 0.6$.

The results represented make it possible to note that the quasiplanar quasilinear theory of cavitation flows of a viscous and capillary fluid can serve to describe streamlined bodies of smooth outlines in the partial cavitation regime.

The authors are grateful to G. Yu. Stepanov for his interest in this study.

LITERATURE CITED

1. V. H. Arakeri, "Viscous effects on the position of cavitation separation from smooth bodies," J. Fluid Mech., 68, 4 (1975).
2. Y. Izumida, S. Tamiya, et al., "The cavitation characteristic of two-dimensional hydrofoils," J. Soc. Nav. Arch. Jpn., 146 (1979).
3. A. N. Ivanov, Hydrodynamics of Evolving Cavitation Flows [in Russian], Sudostroenie, Leningrad (1980).
4. V. H. Arakeri and A. J. Acosta, "Cavitation inception observation on axisymmetric bodies at supercritical Reynolds numbers," J. Ship Res., 20, 40 (1946).
5. E. L. Amromin, "Calculations of cavitation flows of a viscous fluid," Izv. Akad. Nauk SSSR, Mekh. Zhidk. Gaz., No. 6 (1985).
6. L. V. Gogish and G. Yu. Stepanov, Turbulent Separated Flows [in Russian], Nauka, Moscow (1979).
7. E. L. Amromin and A. N. Ivanov, "Determination of the position of separation points of a cavitation cavity from a body with account of fluid viscosity and capillarity," Dokl. Akad. Nauk SSSR, 262, No. 4 (1982).
8. E. L. Amromin, K. V. Aleksandrov, and Yu. L. Levkovskii, "Determination of generation conditions of cavitation on bodies streamlined with separation and an associated boundary layer," Prikl. Mekh. Tekh. Fiz., No. 2 (1986).
9. K. K. Fedyaevskii, A. S. Ginevskii, and A. V. Kolesnikov, Calculations of Turbulent Boundary Layers of Incompressible Fluids [in Russian], Sudostroenie, Leningrad (1973).
10. V. F. Bavin, N. Yu. Zavadovskii, et al., Contemporary Methods of Propeller Calculations [in Russian], Sudostroenie, Leningrad (1983).
11. H. Yamaguchi and H. Kato, "Nonlinear theory for partially cavitating hydrofoils," J. Soc. Nav. Arch. Jpn., 152 (1983).
12. F. Numachi, K. Tsunoda, and I. Chida, "Cavitation tests on hydrofoil profiles of simple form," Rep. Inst. High Speed Mech. Jpn., No. 9 (1959).
13. P. van Oossanen, "Method for the assessment of the cavitation performance of marine propellers," Int. Shipbuilding Progr., 22, No. 245 (1975).